Peering into the rock: a 4D synchrotron study of salt solution movement within masonry sandstone

C. Graham[1], M. Lee[1], V. Phoenix[1] and M. Young[2]
[1]School of Geographical and Earth Sciences, University of Glasgow, U.K
[2]Historic Scotland, Conservation Directorate, Edinburgh, U.K
* c.graham.1@research.gla.ac.uk

Abstract

Here we report results from an initial study on salt solution movement within masonry sandstone. The capillary uptake of 6M calcium iodide solution into Blaxter and Locharbriggs sandstone was imaged by micro computed tomography scanning at three minute intervals. Over a scanning period of seven seconds/360^{o} scan, the solution movement was successfully visualised and quantified. Results show distinct differences in the uptake characteristics of Blaxter and Locharbriggs sandstone. Flow is dominant within permeable layers in the Locharbriggs samples forming thin layers, coating grains that permit the movement of solution without filling pores. It is thought that preferential flow through these confined permeable layers may be an important determinant of salt crystallisation processes.

Keywords: Sandstone, Synchrotron CT Scanning

1 Introduction

The crystallisation of soluble salts is one of the major decay mechanisms affecting sandstone masonry. Salts are introduced into masonry through a number of pathways including (i) capillary rise from de-icing salts, fertilizers and soils saturated into groundwater [1], (ii) inappropriate chemical cleaning methods, (iii) sea spray and air pollution [2,3] and (iv) the alteration and mobilisation of inherent materials such as mortars [4,5]. Salt solution ingress and the subsequent drying pathways are extremely important factors that influence both the location and severity of salt crystallisation. Unsaturated flow dominates the movement of liquid within porous building materials and is controlled by capillary forces. The extent of capillary flow depends on (i) the petrographic properties of the stone, (ii) solution properties, such as surface tension and viscosity and (iii) environmental parameters including temperature and relative humidity (RH). Several salt types have been identified as being major destructive agents within building stone. These include sodium sulphate [6-8], magnesium sulphate [9, 10], gypsum [3] and sodium chloride [9, 11]. Mixtures of salt ions are generally found within buildings, leading to the dynamic crystallisation of many salt types throughout a relatively short space of time [12]. The most damaging mechanisms responsible for damage within natural stone include (i) the thermal expansion of salts [13], (ii) hydration pressures [14] and (iii) crystallisation pressures [15, 16]. Alongside environmental conditions and solution properties, the pore characteristics of the stone influence the uptake and distribution of moisture as well as the rate and magnitude of decay. Both the total connected porosity and distribution of pore sizes, particularly of micropores (<0.1µm) have been shown to be important factors in the generation of high crystallisation pressures [17, 18].

The uptake and crystallisation of salts within building stone is an extremely complex system that contains many variable parameters. The mechanisms by which salts damage building materials cannot be fully understood by invasive sampling and analysis after crystallisation because the key to the process lies in the feedbacks between salt solution movement, salt crystal growth and rock microstructure at the pore scale. A suitable technique in the visualisation of material pore space and recently fluid movement is x-ray micro-computed tomography scanning (µCT). µCT has been used extensively in the fields of geology [19, 20], archaeology [21], palaeontology [22, 23] and cultural heritage [24] to quantify pore space [25-27] and weathering processes [28]. Recent research has made use of synchrotron facilities [29] that allow greater versatility and precision of measurements. Synchrotron µCT and neutron imaging have been used successfully to image and quantify solution movement through sand [30] and limestone [31].

In order to visualise the uptake and movement of salt solution within building stone a non-destructive 4-dimensional µCT study was undertaken using the I12 beamline at the Diamond Light Source synchrotron, UK.

2 Materials and methods

Two sandstones are used within this study, representative of replacement and historic sandstones used through the UK. Petrographic analyses of each rock type took place using transmitted light microscopy and scanning electron microscopy (SEM). The hydric behaviour and subsequent pore system was measured on six repeat samples (6cm^3 cubes) using a range of British Standard tests including: (i) water absorption coefficient (BS EN 13755:2008), (ii) capillary absorption coefficient (BS EN 1925:1999), (iii) saturation coefficient, (iv) effective open porosity by buoyancy weighing (BS EN 1936:2006) and porosity and pore size distribution analysis by helium porosimetry and mercury intrusion porosimetry (MIP).

2.1 Sandstone

Locharbriggs is a red aeolian sandstone of lower Permian age quarried in Dumfries and Galloway, southern Scotland from the oldest and largest red sandstone quarry in Scotland, first quarried in 1759. Locharbriggs is a mineralogically mature, medium grained and poorly sorted sandstone containing abundant clean, sub-rounded –angular quartz grains and a lower percentage of feldspar grains. Grain sizes are variable but contain well established hematite rims throughout. The stone matrix is composed of poorly sorted and broken lithic fragments, quartz grains, smectite clay and weak silica cement. There is a strong and distinguishable fabric throughout the stone that is visible in hand specimen. Layers measure between 1-3mm in thickness and are characterised by small, poorly sorted quartz grains, small Fe-oxides and small, poorly connected pores, separated by thicker layers of larger pores and grains. It has an average porosity of 19.5%, a water absorption coefficient of 9.82% and a capillary coefficient of 309 g/m^2/sec$^{1/2}$. Locharbriggs contains a bimodal distribution of pore sizes, with an average of 50% of pores within the 5µm - 25µm radius range and 9% within the 0.05µm – 0.5µm radius range. Locharbriggs is an extremely important and popular building stone across the UK, with historically important buildings constructed of Locharbriggs dating back to the 1700s. Locharbriggs sandstone has been used extensively in other research looking at (i) building stone cleaning [32], (ii) sandstone weathering [33] and (iii) the mechanical and hydraulic properties of deformation bands [34].

Blaxter is a blonde-buff, medium grained carboniferous sandstone of fluvial origin, quarried in Northumberland, northern England. It is a mineralogically immature sandstone containing a high abundance of feldspar and muscovite grains that are clearly visible in hand specimen. Most grains are sub-angular but of a consistently similar size (180-200µm). Many of the feldspar and muscovite grains show high weathering characteristics and many have decomposed into kaolinite and illite clay. Fe-coatings of quartz and feldspar grains are common, with detritial clays providing secondary cement to silica between the grains. Blaxter has an average porosity of 15.5%, a water absorption coefficient of 6.15% and a

capillary coefficient of 52g/m^2/s$^{1/2}$. Blaxter contains 53.5% of pores within the 1µm - 25µm radius range and 17.6% within the 0.05µm – 0.5µm radius range. Blaxter is widely used throughout the UK for both new builds and as replacement stone in restoration projects.

2.2 Methods

The sandstone samples were cubes with an 8-10mm edge length, and cylinders >10mm height by 8mm diameter. From the data presented in this paper, the Blaxter and one Locharbriggs sample were cut into cubes and the remaining two Locharbriggs samples were cylinders. The experiment set-up consisted of a bespoke cylindrical chamber 110mm in height by 50mm in diameter and constructed from 2mm thick Perspex. It consisted of two sections: a top part containing a small platform that was used to hold sandstone specimens, and a bottom section that was used to house a small reservoir of salt solution. Both parts of the chamber were connected and sealed together using a large, tight rubber band, with small holes drilled into the platform in the upper section to allow the circulation of air and connection with the reservoir in the lower section. The chamber was sealed using a large rubber bung. In all experiments, samples were held in place using moulded foam to ensure their stability during stage rotation.

The initial proposal of work called for a process whereby solution that was contained in a small reservoir in the bottom section of the chamber was transferred by a filter-paper wick to a piece of 1mm thick filter paper situated on the platform in the top section. Salt solutions would then enter the sample via non-forced capillary uptake from the saturated filter-paper. This would provide solution at a rate that allowed for a five minute time interval before solution entered the stone, during which time safety checks and sample stage positioning could take place. Due to poor contrast between the solution and stone at low solution concentrations, a 6M concentrated calcium iodide (CaI_2) solution, as has been used previously in other similar studies [31], was chosen to ensure sufficient contrast. At this high concentration however, wicking between the lower reservoir and the filter paper prior to safety checks did not take place. In order to solve this problem, pre-saturated filter-paper was used. This provided a second problem as by the time scanning was initiated capillary intrusion into the sample had already started. This meant that the field of view had to be moved to a higher position on the sample to enable fluid movement through the stone to be imaged.

Dynamic, high speed tomography scanning was performed on the I12 beamline at the Diamond Light Source synchrotron, Oxfordshire, UK. Images were captured using module 2 of the Phantom v7.3 camera. This had a field of view of 9.8mm by 7.3mm and a resolution of ~12µm/pixel. With this arrangement the sample stage rotation was set as to ensure that one 360^o scan took only seven seconds to complete and therefore the dynamic movement of solution into and throughout the sample could be

imaged. Five hundred and eighty projections were captured in each 360^{o} scan; however specific images from either the start or end of each scan were omitted due to poor definition of phase boundaries. Unlike conventional laboratory CT scanners, synchrotron radiation is generated by the movement of electrons as they pass through magnetic fields at close to the speed of light. As these electrons are steered through the magnetic fields they lose energy in the form of synchrotron light. This light is harnessed and subsequently filtered and focused, with the subsequent x-rays used for a number of scientific applications. This results in faster scanning of a better signal-noise ratio than lab based CT systems.

Reconstructed scans were visualised in Avizo 7 software. Each scan was placed through two filters to enhance contrast between greyscale phases and to enhance the edge detection of each separate phase. By using the greyscale distribution of each scan, grain, pore and solution phases were separated and quantified to provide the porosity and solution values through each slice. Each separate scan was then registered to a reference scan to ensure each scan was aligned in each scan set. In order to visualise the change in solution movement from two neighbouring scans, the arithmetic tool was used to calculate the difference between each scan. The resulting difference field was used to visualise and quantify the movement of solution between scans. Some samples were also cropped prior to any analysis to eliminate background “porosity” from out-with the sample.

3 Results

Four individual scan-sets will be discussed in this section. One set from a Blaxter sample (B) and the following three sets from three individual Locharbriggs samples (L1, L2 and L3). Samples B and L1 are scans from cropped cubic samples and samples L2 and L3 from small cores.

3.1 Blaxter (B)

A 3-dimensional visualisation of the open pores, solution and stone grains and a cropped horizontal cross section through the middle of this block are shown in Fig 1. It shows a high percentage of filled pores with sporadic empty porosity of different pore sizes located between larger clusters of solution. Solution within this sample fills a range of pore sizes, likely the most open and accessible pores as highlighted in Fig 1B. Solution does not follow any petrographic structures within the sample and highlights a well distributed range of pore connectivity within the stone. Due to problems associated with the rapid rate of solution uptake, this was the only scan suitable for analysis and therefore does not provide an initial "dry" scan for comparison.

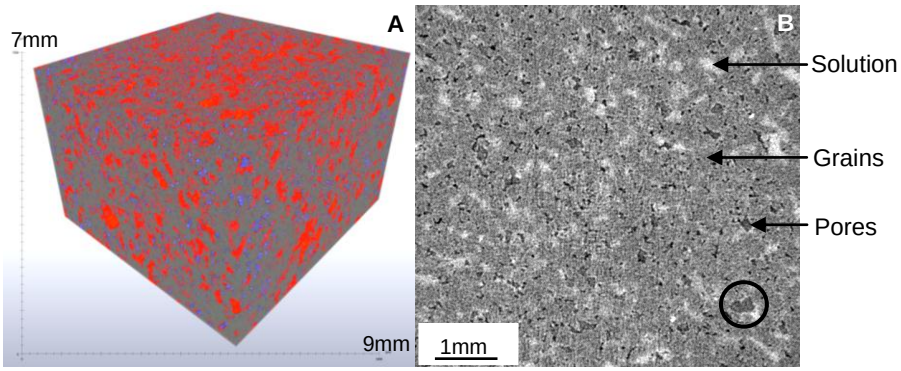

Figure 1: A: 3D visualisation of pores (blue), solution (red) and stone grains (grey). B: 2D cropped horizontal cross section showing each distinct phase. Black circle shows partial ingress of solution into an empty pore, with a white halo at the edge of the pore.

3.2 Locharbriggs 1 (L1)

Seven scans were acquired at three minute intervals. The volumes of solution, porosity, quartz/feldspar grains and Fe-oxides are segmented and calculated at each time interval. The initial porosity values throughout the sample show an average of ~ 17%, which shows little variation throughout the height of the sample. The sample was subject to capillary uptake experiments parallel to bedding. The data show that solution ingress and subsequent transport through the stone is significantly influenced by the internal pore structure, specifically in relation to pore size distributions and the internal fabric (ie bedding) of the stone. The solution transport is restricted to one half of the sample, separated from the rest of the sample by the bedding horizon and a change in mineralogical texture. Porosity in this other, separated layer is significantly lower and less well connected than the coarser layer, thus inhibiting solution penetration. It is likely that this solution has hydraulic connectivity throughout the height of the sample. Initial solution ingress is restricted to a small section in the centre of the coarse layer.

Graph 1 shows the solution volume distribution throughout the sample at each three minute interval. It reveals a steady increase of solution volume height reached by capillary rise in the sample and total solution volume. A noticeable peak is evident around 1.032mm in height from twelve minutes onwards. Solution volumes below this height appear very similar, with little fluctuation as to suggest that most of the accessible pores below this point have been filled by twelve minutes. Open pores below this height in the 9, 12, 15, 18 and 21 minute scans shows that saturation has not been met however. Rather than solution moving through the sample by consecutively filling pores, the solution instead moves through the sample by coating and “wetting” grains. In this process, solution uptake is highly influenced by the viscosity and surface tension of the solution. From twelve minutes onwards, vertical solution movement above 1.032mm is supplied by solution already within the sample at a rate equal to solution ingress into the base of the stone. This would ensure that pores below 1.032mm would not become filled and solution volume below this height would remain stable. From both the visualisation of solution at each time step within the stone and from graph 1, it can be seen that lateral dispersion of solution is more prominent within the first nine minutes of solution uptake. From twelve minutes onwards capillary rise of solution becomes prominent.

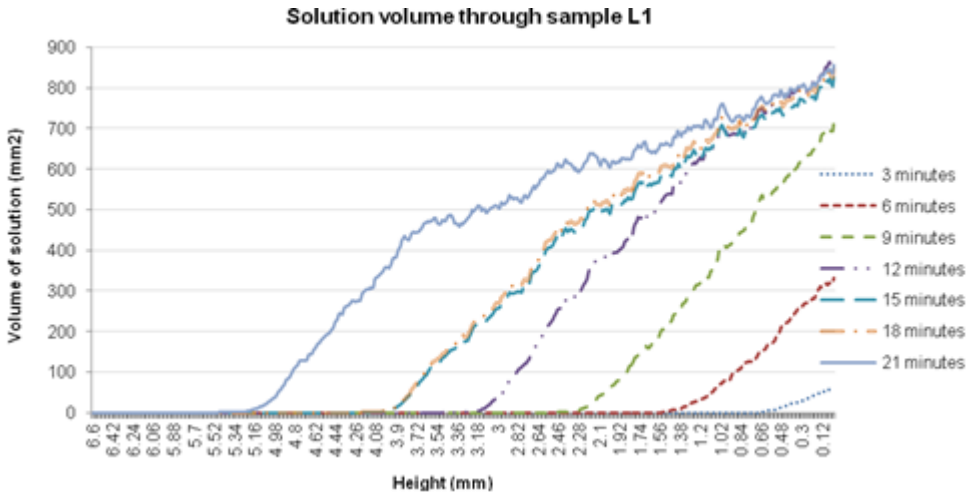

Graph 1: Solution volume per slice through sample L1 at different time periods

From solution visualisation at each time step it is shown that the wetting front is not laterally consistent, with a leading ridge of solution at the centre of the volume (Fig 2). This is in contrast to analysis of B1, whereby solution moves through the sample in individual channels as opposed to homogeneous flow with a defined wetting front.

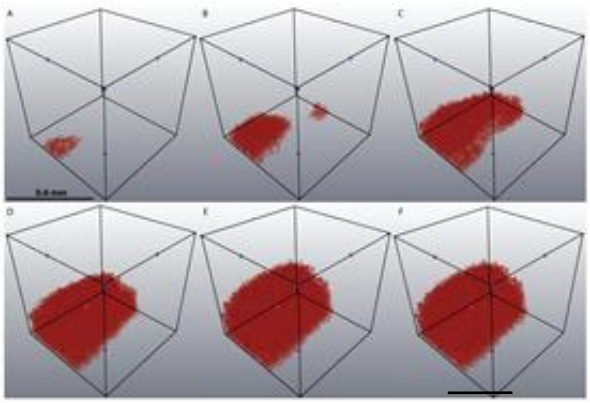

Figure 2: Solution movement through sample L1. A= 3minutes, B= 6minutes, C= 9minutes, D= 12minutes, E= 15minutes, F= 21minutes.

3.3 Locharbriggs 2 (L2)

Sample L2 is a scan of the upper 7mm (Fig 3A) of the sample due to problems associated with the rapid uptake of solution and so does not represent the initial ingress of solution into the stone. Unlike sample L1, Fig 3 shows evidence of complete pore filling in sample L2. The black boxes highlight the infilling of a pore with solution over the full period of scanning. The solution does not neatly "outline" the shape of the pore but instead is imaged within the pore and pore-throats that are undetected at this resolution. The red circles highlight the partial infilling of a smaller pore whereby the solution adheres to the surrounding grain surfaces due to capillary forces. These capillary forces will allow the flow of solution throughout the pore network, in which pores are hydraulically connected through this thin solution layer. Fig 4 shows a 3D visualisation of a cropped section within sample L2 of the same time frames as highlighted in Fig 3.

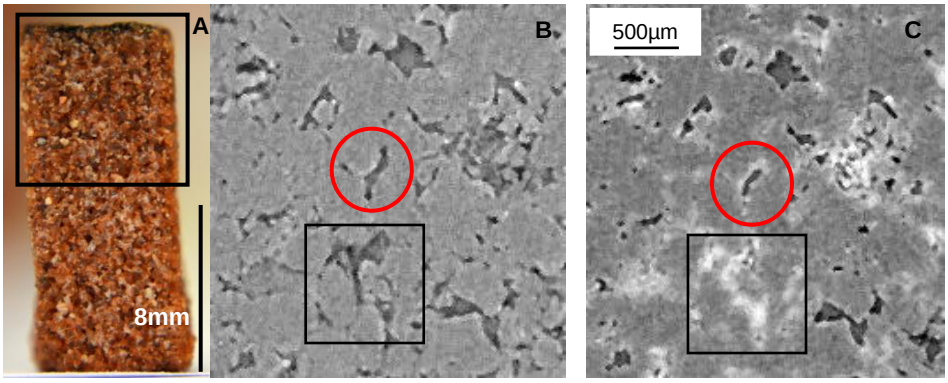

Figure 3: A: Black box highlights the scanned area of L2. B+C: 2D images of L2. Black boxes highlight the infilling of a pore. Red circles highlight the partial infilling of a pore. B: Initial scan. C: Final scan (approximately 15minutes later).

It is clearer to see the infilling of the pore network in Fig 4, whereby the segmentation of solution in Fig 4B helps to define smaller pore-throats that are not detected otherwise. Fig 4A shows that solution moves through the rock by capillary action, adhering to the grain surfaces while staying in hydraulic connectivity with the larger solution volume present at lower levels within the sample. Larger pores at this height are not completely filled with solution over this short scanning period. Graph 2 shows the change in porosity values through the cropped section visualised in Fig 4. It shows the natural variation of porosity within the Locharbriggs sandstone as highlighted by the high porosity peaks at slice numbers 39, 108 and 138. It shows that at the start of scanning some of the porosity of the lower slices were already partially filled. The infilling of porosity is

clearly shown, especially over the first six minutes of scanning. From six to nine minutes the change in unfilled porosity over each slice is compressed and shows greater evidence of the infilling of pore throats (that aren't counted in porosity values) and the capillary rise of solution, whereby only the partial filling of pores takes place due to greater capillary forces causing the vertical transportation of solution.

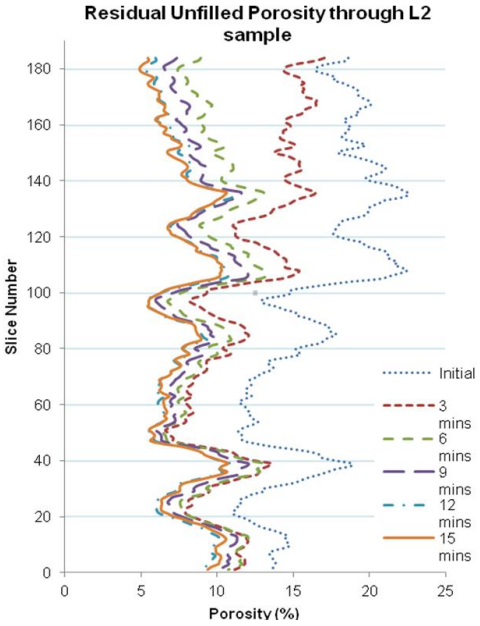

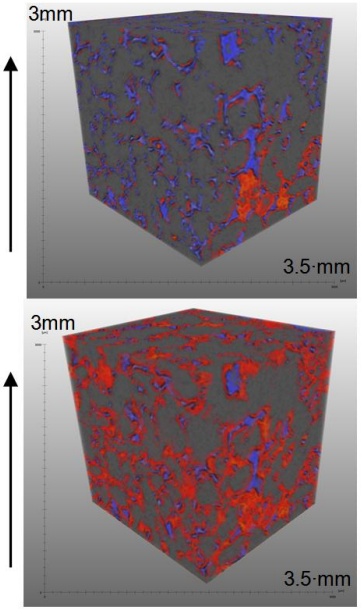

Graph 2: Porosity measurements through the cropped section Fig 4.

Figure 4: Visualisation of porosity (blue), solution (red) and grains (grey). Black arrow shows direction of fluid movement. A: Initial scan showing partial infilling of large pore network and grains coating within other pores allowing solution movement through the pore network. B: The final scan (15minutes from the initial scan) showing pore infilling and highlighting narrow pore throats that weren't initially detected.

3.4 Locharbriggs 3 (L3)

Sample L3 represents the scan of the upper 7mm of the sample, similar to L2. It shows a similar process of fluid movement, whereby the flow is concentrated within more permeable bedding planes of the stone. Preferential solution movement takes place near the edges of stone and within bedding planes of the stone. The visualisation of differences between neighbouring scans highlights the lack of horizontal flow. From

the visualisation of pores that have lost fluid it indicates that the rate of vertical, capillary flow is not constant throughout the full section. If this was true then there would be no loss of solution in the feeder pores as they would be continually filled as solution moved through them, penetrating the open pores above.

4 Discussion

Analysis of four samples from two sandstone types has shown that the uptake characteristics and flow through each of these sandstone types differs significantly. Specifically, the mechanisms by which solution is absorbed and transferred through the stone are comparable, however the distribution of solution within the stone is different and is influenced by pore structure. An interesting and important result from analysis of Locharbriggs sandstone regards the preferential solution uptake and movement through confined permeable layers that was evident in all Locharbriggs samples. This may be an important determinant of salt crystallisation processes. The drying of sandstone is a complex and extremely important factor that significantly influences the distribution and damage potential of salt crystallisation. Damaging crystallisation pressures can develop during this drying process. Drying is influenced by solution properties, the pore network and surface modifications such as biological growth and hard surface crusts. The margin between permeable and impermeable layers in the Locharbriggs samples (specifically L1) presents a boundary in pore size distributions and a potential barrier for hydraulically controlled drying. This would lead to a vapour dominated drying regime, whereby the drying front would be located at the boundary, leading to salt crystallisation. This process could result in the preferential crystallisation of salts within a small layer within the stone. The distribution of high crystallisation pressures extending over such an area could lead to the development of fracture chains and scaling decay processes.

5 Conclusions and future work

The movement of 6M concentrated CaI_2 solution was successfully imaged in one sample of Blaxter sandstone and three samples of Locharbriggs sandstone over a period of ~21minutes. Over a scanning period of seven seconds, it was possible to image the grains, pore structure and salt solution within the samples. From repeated scans over three minute intervals the change in solution volume and porosity was visualised and calculated. Differences between neighbouring scans also allowed the visualisation and quantification of solution change within the stone. Images from the Blaxter sample show that the solution is well distributed within the stone, filling pores, while other, possibly disconnected pores remain unfilled. Solution distribution isn't influenced by any obvious structural features of the stone. Rather, it is likely influenced by the random distribution of pore sizes. All three Locharbriggs samples showed

similar fluid flow characteristics whereby more permeable layers permitted preferential flow through the stone. Vertical capillary uptake was the dominant flow mechanism, with thin solution films that coated grains evident in the L2 sample. This preferential flow within certain layers may influence the location and subsequent intensity of salt crystallisation during the drying stage of the stone.

An important issue that must be acknowledged is the effect of such a highly concentrated CaI_2 solution on fluid dynamics within the sandstones. In order to enable sufficient contrast between solution and the rock, and after several attempts at lower concentrations, a 6M concentration was accepted. This significantly increased the viscosity and the surface tension of the solution. This would impact on the fluid dynamics and influence the flow rate and accessibility into certain pore sizes. It was with this issue and problems associated with the experimental design that no attempt to calculate fluid flow rate were made. This increase in contrast did however allow the visualisation of pore-throats to be made that were otherwise undetected. It highlighted that pore throats were preferentially filled while larger pores remained partially filled.

Results from this study demonstrate that synchrotron X-ray µCT is a useful and valuable tool in the non-destructive analysis of building materials, specifically in the continued research of fluid flow dynamics in porous materials. It shows that with an extremely simple set-up, high quality data can be produced. It is believed that this study serves as a starting point for further research of salt crystallisation processes in building materials using dynamic synchrotron techniques. Advances would include the increased speed of imaging, an increased data set of stones containing contrasting pore structures and research of the drying regimes experienced by these sandstone types. Further study must strive to use more realistic solution concentrations as to replicate, as close as possible, natural conditions.

Acknowledgements

Thanks are extended to Robert Atwood and Nghia Vo of the I12 beamline at Diamond Light Source and to Kate Dobson of the Manchester X-ray Imaging Facility for their assistance and advice both during and after the experimental work. Thanks are also extended to Alison Wright and Emma Fairley of The University of Glasgow for their help and assistance during the allocated beamtime at Diamond, as part of a four person team and for supplying samples L2 and L3.

References

[1] Charola, E. A. “Salts in the deterioration of porous materials: An overview.” Journal of the American Institute for Conservation (39) Number 3, Article 2. (2000) 327 – 343.

[2] Cardell, C. Delalieux, F. Roumpopoulos, K. Moropoulou, A. Auger, F. and Van Grieken, R. “Salt-induced decay in calcareous stone monuments and buildings in a marine environment in SW France” Construction and Building Materials (17) (2003) 165 – 179.

[3] Lubelli, B. van Hees, R. P.J. and Groot, C. J. W. P. “The role of sea salts in the occurrence of different damage mechanisms and decay patterns on brick masonry” Construction and Building Materials (18) (2004) 119 – 124.

[4] Perry, S.H. and Duffy, A.P. “The Short-term effects of mortar joints on salt movement in stone” Atmospheric Environment (31) (1996) 1297 – 1307.

[5] Ruedrich, J. and Siegesmund, S. “Salt and ice crystallisation in porous sandstones” Environmental Geology (52) (2007) 225 – 249.

[6] Rodriguez-Navarro, C. Doehne, E. and Sebastian, E. “How does sodium sulphate crystallize? Implications for the decay and testing of building materials” Cement and Concrete Research (30) (2000) 1527-1534.

[7] Espinosa, R.M. Franke, L. and Deckelmann, G. “Model for the mechanical stress due to the salt crystallization in porous materials” Construction and Building Materials (22) (2008) 1350 – 1367.

[8] Espinosa-Marzal, R.M. and Sherer, G.W. “Mechanisms of damage by salt” Geological Society, London, Special Publications (331) (2010) 61-77.

[9] Lopez-Arce, P. Doehne, E. Greenshields, J. Benavente, D. and Young, D. “Treatment of rising damp and salt decay: the historic masonry buildings of Adelaide, South Australia.” Materials and Structures (41) (2009) 827 – 848.

[10] Balboni, E. Espinosa-Marzal, R. M. Doehne, E. and Scherer, G. W. “Can drying and re-wetting of magnesium sulphate salts lead to damage of stone?” Environmental Earth Science (63) (2011) 1463 – 1473.

[11] Ruedrich, J. Seidel, M. Rothert, E. and Siegesmund, S. “Length changes of sandstones caused by salt crystallization.” Geological Society, London, Special Publications (271) (2007) 199 – 209.

[12] Zehnder, K. and Schoch, O. “Efflorescence of mirabilite, epsomite and gypsum traced by automated monitoring on-site.” Journal of Cultural Heritage (10) (2009) 319-330.

[13] Al-Naddaf, M. “The effect of salts on thermal and hydric dilation of porous building stone” Archaeometry (51) (2009) 495-505.

[14] Flatt, Robert. J. “Salt damage in porous materials: how high supersaturations are generated” Journal of Crystal Growth (242) (2002) 435 – 454.

[15] Theoulakis, P. and Moropoulou, A. “Salt Crystal Growth as Weathering Mechanism of Porous Stone on Historic Masonry” Journal of Porous materials (6) (1999) 345 – 358.

[16] Scherer, G. W. “Stress from crystallization of salt” Cement and concrete research (34) (2004) 1613 – 1624.

[17] Buj, O. and Gisbert, J. “Influence of pore morphology on the durability of sedimentary building stones from Aragon (Spain) subjected to standard salt decay tests” Environmental Earth Science (61) (2010) 1327 – 1336.

[18] Yu, S. and Oguchi, C.T. “Role of pore size distribution in salt uptake, damage, and predicting salt susceptibility of eight types of Japanese building stones” Engineering Geology (115) (2010) 226 – 236.

[19] Snelling, A.M. Zalasiewicz, Jan. A. and Reeds, I. “Using X-ray images to analyse graptolite distribution and alignment in Welsh mudrocks.” Proceedings of the Yorkshire Geological Society (58) (2010) 129 – 140.

[20] Needham, A. W. Abel, R. L. Tomkinson, T. and Grady, M. M. “Martian subsurface fluid pathways and 3D mineralogy of the Nakhla meteorite.” Geochimica et Cosmochimica Acta (116) (2013) 96 – 110.

[21] Hiller, J. C. and Wess, T. J. “The use of small-angle X-ray scattering to study archaeological and experimentally altered bone.” J. Archaeol. Sci 33 (4) (2006) 560 – 572.

[22] Clark, N. D. L. Adams, C. Lawton, T. Cruickshank, A. R. I. and Woods, K. “The Elgin marvel: using magnetic resonance imaging to

look at a mouldic fossil from the Permian of Elgin, Scotland, UK." Magnetic Resonance Imaging (22) (2004) 269 – 273.

[23] Douarin, M. Sinclair, D. J. Elliot, Mary. Henry, L. Long, D. Mitchison, F. and Roberts, J.M. "Changes in fossil assemblage in sediment cores from Mingulay Reef Complex (NE Atlantic): Implications for coral reef build-up." Deep-Sea Research II (99) (2014) 286 – 296.

[24] Rozenbaum, O. "3-D characterization of weathered building limestones by high resolution synchrotron X-ray microtomography." Science of the Total Environment (409) (2011) 1959 – 1966.

[25] Cnudde, V. Cwirzen, A. Masschaele, B. And Jacobs, P. J. S. "Porosity and microstructure characterization of building stones and concrete" Engineering Geology (103) (2009) 76 – 83.

[26] Long, H. Swennen, R. Foubert, Anneleen. Dierick, M. and Jacobs, P. "3D quantification of mineral components and porosity distribution in Westphalian C sandstone by microfocus X-ray computed tomography." Sedimentary Geology (220) (2009) 116 – 125.

[27] Cnudde, V. Dewanckele, J. Boone, M. De Kock, T. Boone, M. Brabant, L. Dusar, M. De Ceukelaire, M. De Clercq, H. Hayen, R. and Jacobs, P. "High-Resolution X-Ray CT for 3D Petrography of Ferruginous Sandstone for an Investigation for Building Stone Decay." Microscopy Research and Technique (74) (2011) 1006 – 1017.

[28] Dewanckele, J. De Kock, T. Boone, M. A. Cnudde, V. Brabant, L. Boone, M. N. Fronteau, G. Van Hoorebeke, L. and Jacobs, P. "4D imaging and quantification of pore structure modifications inside natural building stones by means of high resolution X-ray CT." Science of the Total Environment (416) (2012) 436 – 448.

[29] Derluyn, H. Dewanckele, J. Boone, M.N. Cnudde, V. Derome, D. and Carmeliet, J. "Crystallization of hydrated and anhydrous salts in porous limestone resolved by synchrotron X-ray microtomography." Nuclear Instruments and Methods in Physics Research B (324) (2014) 102 – 112.

[30] Shokri, N. Lehmann, P. and Or, D. "Liquid-phase continuity and solute concentration dynamics during evaporation from porous media: Pore-scale processes near vapourization surface." Physical Review (81) (2010) 1 – 7.

[31] Dewanckele, J. De Kock, T. Fronteau, G. Derluyn, H. Vontobel, P. Dierick, M. Van Hoorebek, L. Jacobs, P. and Cnudde, V. “Neutron radiography and X-ray computed tomography for quantifying weathering and water uptake processes inside porous limestone used as building material.” Materials Characterization (88) (2014) 86 – 99.

[32] Young, M. E. Urquhart, D. C. M. and Laing, R. A. “Maintenance and repair issues for stone cleaned sandstone and granite building façades.” Building and Environment (38) (2003) 1125 – 1131.

[33] McCabe, S. Smith, B. J. McAllister, J. J. Gomez-Heras, M. McAllister, D. Warke, P, A. Curran, J. M. and Basheer, A. M. “Changing climate, changing process: Implications for salt transportation and weathering within building sandstones in the UK.” Environmental Earth Sciences (69) (2013) 1225 – 1235.

[34] Main, I, Mair, K. Kwon, Ohmyoung. Elphick, S. and Ngwenya, B. “Experimental constraints on the mechanical and hydraulic properties of deformation bands in porous sandstones: a review” Geological Society, London, Special Publications (186) (2001) 43 – 63.